Supporting Information

Organic-Inorganic Complex S-Scheme Photocatalyst Resorcinol-Formaldehyde Resins/$Bi_2O_2CO_3$ with Enhanced Photocatalytic H_2O_2 Production

Meichao Gao*[a], Jianting Wang[a], Huichao Cui[a], Mingyang Meng[a], Yuanyuan Feng*[a], Yunyun Gong[a], Changlong Sun*[b]

[a]Key Laboratory of Catalytic Conversion and Clean Energy in Universities of Shandong Province, School of Chemistry and Chemical Engineering, Qufu Normal University, Qufu 273165, Shandong, P. R. China

[b]College of Materials Science and Engineering, Qingdao University of Science and Technology, Qingdao 266042, Shandong, P. R. China

Corresponding author.

E-mail address: meichaogao@hotmail.com (M. Gao); fengyy@qfnu.edu.cn (Y. Feng); changlongsun@qust.edu.cn (C. Sun).

1.1. Chemical materials

All chemicals and reagents were of analytical grades and used without further purification. Bismuth nitrate pentahydrate ($Bi(NO_3)_3·5H_2O$, 99%), nitric acid (HNO_3, 67%), sodium carbonate (Na_2CO_3, 99.8%), cetyltrimethylammonium bromide ($C_{19}H_{42}BrN$, 99%), formaldehyde (HCHO, 38%), resorcinol ($C_6H_6O_2$, 99%), ammonia solution ($NH_3·H_2O$, 25~28%), absolute ethyl alcohol (C_2H_5OH, 99.8%), isopropanol (C_3H_8O, 99.9%), para-benzoquinone ($C_6H_4O_2$, 99%), potassium ferricyanide ($K_3[Fe(CN)_6]$, 99%), methyl alcohol (CH_3OH, 99%), anhydrous sodium sulfate (Na_2SO_4, 99%), ammonium molybdate tetrahydrate ($(NH_4)_6Mo_7O_{24}$, 99%) and potassium iodide (KI, 99%) were purchased from Shanghai Sinopharm Chemical Reagent Co., Ltd, China.

1.2. Experimental

The RF/$Bi_2O_2CO_3$ composites were fabricated using the electrostatic self-assembly method. First, $Bi_2O_2CO_3$ was prepared based on our previous work[1]. A certain mass of $Bi_2O_2CO_3$ was dispersed into an ethanol-water mixed solution with a volume ratio of 6:4. Then, 0.7 g resorcinol, 0.5 mL formaldehyde solution, and 2 g cetyltrimethylammonium bromide (CTAB) were added to the mixed solution. The mixture was kept stirring at room temperature for 24 hours. Then, 1 mL of ammonia solution was added to the mixed solution and stirred for 15 minutes. The resulting solid was collected by centrifugation, washed several times with deionized water and ethanol, and dried in an oven at 60°C for 12 h. The obtained powder was denoted as RF/$Bi_2O_2CO_3$-X ($Bi_2O_2CO_3$ is BOC and X is the mass of $Bi_2O_2CO_3$). The pure RF (resorcinol-formaldehyde resins) was synthesized according to previous work[2].

1.3. Characterization

X-ray diffraction (XRD) patterns were recorded by a diffractometer (D8 Advance, Bruker Co., Germany) with Cu K_α-irradiation operated at 40 kV and 30 mA. Sample morphologies were observed by a JSM-6700F scanning electron microscope (SEM). Transmission electron microscopy (TEM, JEM-2100 instrument, JEOL Ltd., Japan) was performed to gain morphology and crystalline structure information of samples. X-ray photoelectron spectra (XPS) were collected by an X-ray photoelectron spectrometer (Kratos Axis Ultra). The absorption spectra and diffuse reflection spectra of

samples were characterized using an ultraviolet-visible spectrophotometer (TU-1901, Beijing Puxi General Instrument). The photoelectrochemical property was tested using a CHI760E electrochemical workstation in Na_2SO_4 solution (0.5 M, pH=7) with a three-electrode system: Ag/AgCl reference electrode, Pt plate counter electrode. FTO supporting photocatalyst was a working electrode and a 300 W Xenon lamp was employed as the light source. The pulse chemisorption experiment was conducted using a Micromeritics Autochem II 2920 Chemisorption Analyzer equipped with a TCD detector. In the pulse experiments, the sample was initially heated to 120 °C under a helium (He) flow for one hour to cleanse the surface, before being cooled to 50 °C. A continuous pulse of 4% O_2 in helium was introduced and measured until adsorption saturation was reached.

1.4. Computational method

We have employed the Vienna Ab Initio Simulation Package (VASP)[3,4] to perform all the density functional theory (DFT) calculations within the generalized gradient approximation (GGA) using the PBE[5] formulation. We have chosen the projected augmented wave (PAW) potentials[6,7] to describe the ionic cores and take valence electrons into account using a plane wave basis set with a kinetic energy cutoff of 400 eV. Partial occupancies of the Kohn−Sham orbitals were allowed using the Gaussian smearing method and a width of 0.05 eV. The electronic energy was considered self-consistent when the energy change was smaller than 10−5 eV. A geometry optimization was considered convergent when the force change was smaller than 0.02 eV/Å. Grimme's DFT-D3 methodology[8] was used to describe the dispersion interactions.

The equilibrium lattice constants of the orthorhombic Bi_2CO_5 unit cell were optimized to be a=5.468 Å, b=27.395 Å, c=5.440 Å. We then use it to construct a Bi_2CO_5 (110) surface model with p (6×1) periodicity in the X and Y directions and 1 stoichiometric layer in the Z direction separated by a vacuum layer in the depth of 15 Å in order to separate the surface slab from its periodic duplicates. This Bi_2CO_5 (110) model 1 comprises 96 Bi, 48 C, and 240 O atoms. An RF linear chain with 5 units was on it. During structural optimizations, the Γ point in the Brillouin zone was used for k-point sampling, and the bottom half stoichiometric layer of Bi_2CO_5 (110) was fixed while the rest were allowed to relax.

1.5. Photocatalytic production of H_2O_2

Typically, 20 mg of the photocatalyst was dissolved in the mixture of deionized water (45 mL) and CH_3OH (5 mL) and ultrasonicated for 10 min. Then the solution was put in a dark box and magnetically stirred, meanwhile, the solution was bubbled with air for 30 min. Then the photocatalytic reaction was performed under simulated solar illumination by using a 300 W Xenon lamp for 1 h at room temperature. Finally, 5 mL of solution was taken out by syringe and then filtered with an MCE filter membrane to separate photocatalysts for further testing. The production of H_2O_2 was detected by the typical iodometry method. Briefly, 50 μL of 0.01 mol L^{-1} $(NH_4)_6Mo_7O_{24}$ aqueous solution and 2 mL of 0.1 mol L^{-1} potassium iodide (KI) aqueous solution was added to 5 mL of filtrate, which was then kept for 10 min. The H_2O_2 molecules reacted with iodide anions (I^-) under acidic conditions to produce I_3^- anions, which exhibit a strong optical absorption at 352 nm. The amount of I_3^- was analyzed by UV–visible spectroscopy from which the amount of H_2O_2 was subsequently calculated. The standard curve for H_2O_2 is shown in Fig. S1.

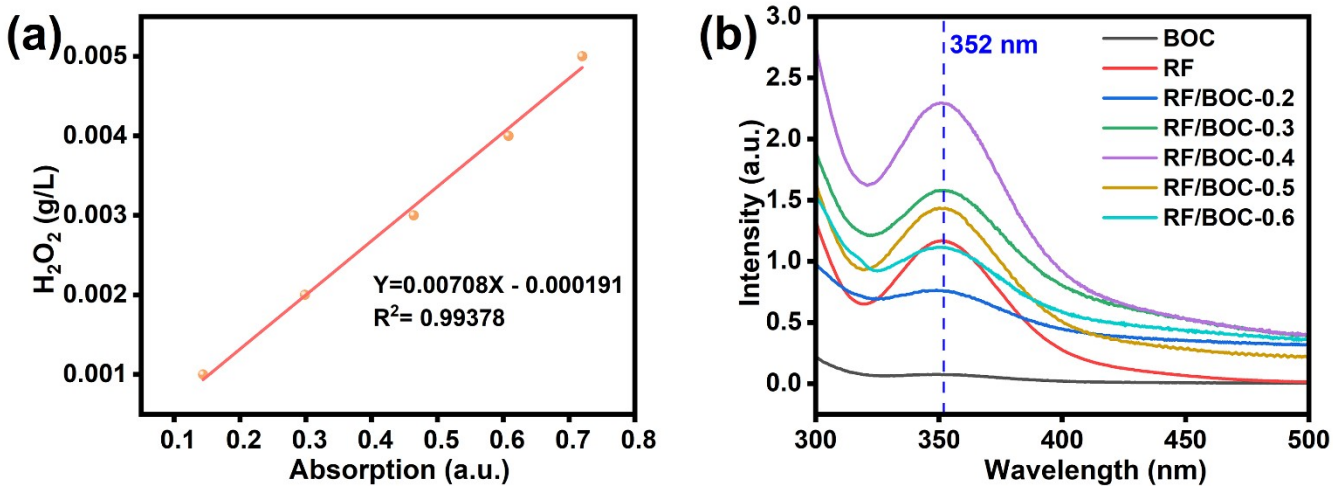

Fig. S1. (a) The standard curve of H_2O_2 production; (b) UV-vis absorption spectra of photocatalysis H_2O_2 production by RF/BOC-X (X= 0.2, 0.3, 0.4, 0.5, and 0.6 g).

1.6. Results Section

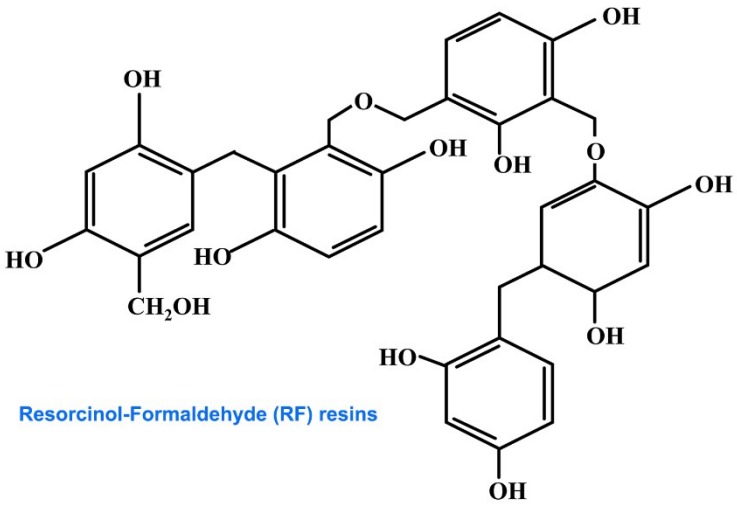

Fig. S2. Structural chemical formula diagram of resorcinol formaldehyde resin.

As illustrated in Fig. S2, a structural formula diagram of resorcinol formaldehyde resin is provided. Numerous phenolic hydroxyl groups can be observed surrounding the resorcinol formaldehyde resin structure[9-11]. The presence of the phenol hydroxyl group makes the binding with BOC have a close contact heterojunction interface. In addition, the phenolic hydroxyl groups in RF have a positive significance for the production of active sites of reactive oxygen species and the stability of intermediates.

We have calculated the crystallite size of BOC crystal using the Scherrer equation and investigated the potential strain effects of the material. The crystallite size of BOC crystal was estimated by employing the Scherrer equation given below[12]:

$$D = \frac{0.89\lambda}{\beta_{hkl}\cos\theta}$$

where D denotes the crystallite size, λ represents the Cu-K_α source wavelength (0.15406 nm), β_{hkl} corresponds to the full width at half maximum (FWHM) in radian of the (hkl) plane, and θ is the diffraction angle. Both the crystallite size and micro-strain have significant effects on the FWHM. By comparing the widths and positions of the observed diffraction peaks with those of standard peaks, we anticipate that the influence of micro-strain is relatively minor, with the crystallite size being the primary factor determining peak width. Based on the behavior of the main lattice plane (013), the crystallite size of BOC was estimated to be 19.22 nm, indicating good crystallinity.

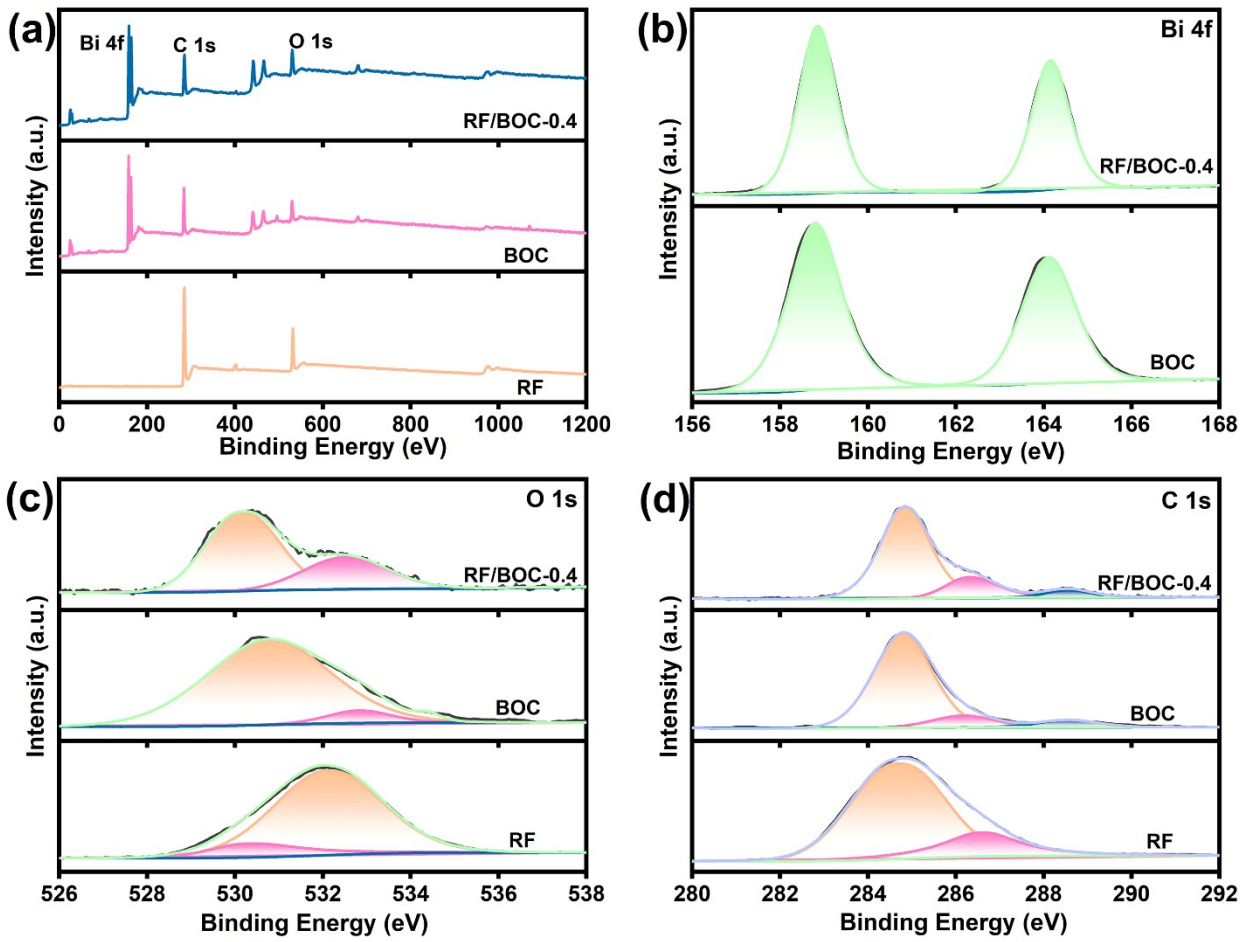

Fig. S3. (a) The XPS spectra of RF, BOC, and RF/BOC-0.4; the high-resolution XPS spectra of (b) Bi 4f, (c) O 1s, (d) C 1s.

XPS analysis was performed to examine the surface composition and chemical states of the relevant elements[13]. As shown in the survey spectrum (Fig. S3a), the presence of Bi, O, and C elements was verified. High-resolution XPS spectra for the Bi 4f region are presented in Fig. S3b. In the RF/BOC-0.4 sample, the peaks observed at 158.9 and 164.2 eV correspond to Bi $4f_{7/2}$ and Bi $4f_{5/2}$, respectively. Compared to pure BOC, the Bi 4f peaks in the RF/BOC-0.4 samples show a shift to higher binding energies, indicating the transfer of electrons from BOC to RF. The analysis of elements C and O is presented in Fig. S3c and Fig. S3d. In the XPS spectrum of RF, the two prominent peaks at 284.8 and 286.6 eV correspond to C–C and C–O bonds, respectively, which are characteristic of carbon in composite resorcinol–formaldehyde resins.

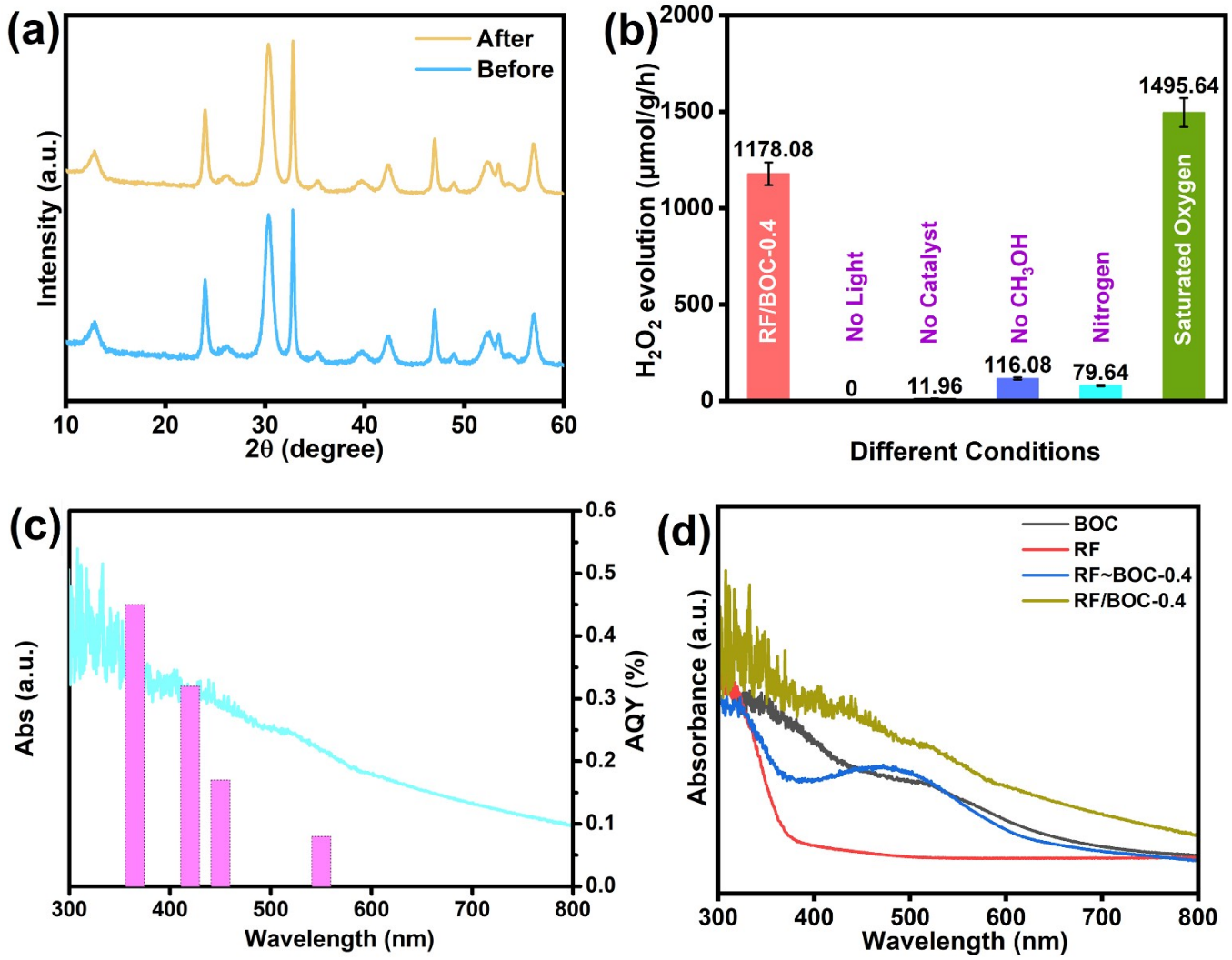

Fig. S4. (a) The XRD patterns after cycling; (b) the average H_2O_2 production rate by RF/BOC-0.4 under different conditions; (c) AQY of RF/BOC-0.4 at different single light wavelengths and (d) The DRS spectrum of the RF, BOC, RF/BOC-0.4 and RF~BOC-0.4 (physical mixture of RF and BOC).

A series of control experiments were conducted to identify the key factors influencing the photocatalytic H_2O_2 performance of the RF/BOC-0.4 catalyst (Fig. S4b). It is evident that the absence of either the catalyst or light significantly reduces H_2O_2 production, indicating that both components are crucial for the effectiveness of photocatalytic systems[14]. However, variations in oxygen concentration reveal a positive correlation with H_2O_2 production. This suggests that hydrogen peroxide generation is reliant on the oxygen reduction reaction. In addition, the lack of methanol also reduces hydrogen peroxide production, which may be attributed to the rapid recombination of electrons with holes[15]. The solar-to-chemical conversion efficiency (SCC%) of RF/BOC-0.4 for H_2O_2 production was determined by using an

equation[16]. According to the equation, the SCC efficiency is calculated to be 0.03%. The energy conversion efficiency of RF/BOC-0.4 was also determined by calculating its apparent quantum yield (AQY)[17]. The transmission spectrum of the bandpass filter employed has been previously documented in the literature[2]. The AQY values for RF/BOC-0.4 at wavelengths 365, 420, 450, and 550 nm were found to be 0.45%, 0.32%, 0.17%, and 0.08%, respectively (Fig. S4c). The physical mixture of RF and BOC was prepared according to the same component content. We performed diffuse reflectance spectroscopy (DRS) tests of the mixture. Through comparison, it has been found that RF/BOC-0.4 exhibits a significant enhancement in light absorption (Fig. S4d), which demonstrated the enhancement of light absorption in RF/BOC-0.4. Thus, the increase of visible-light absorption of RF/BOC-0.4 compared with RF can be attributed to the interfacial interaction with the formation of heterojunctions. This indicates the role of the interface in enhancing light absorption, which contributes to improving photocatalytic activity.

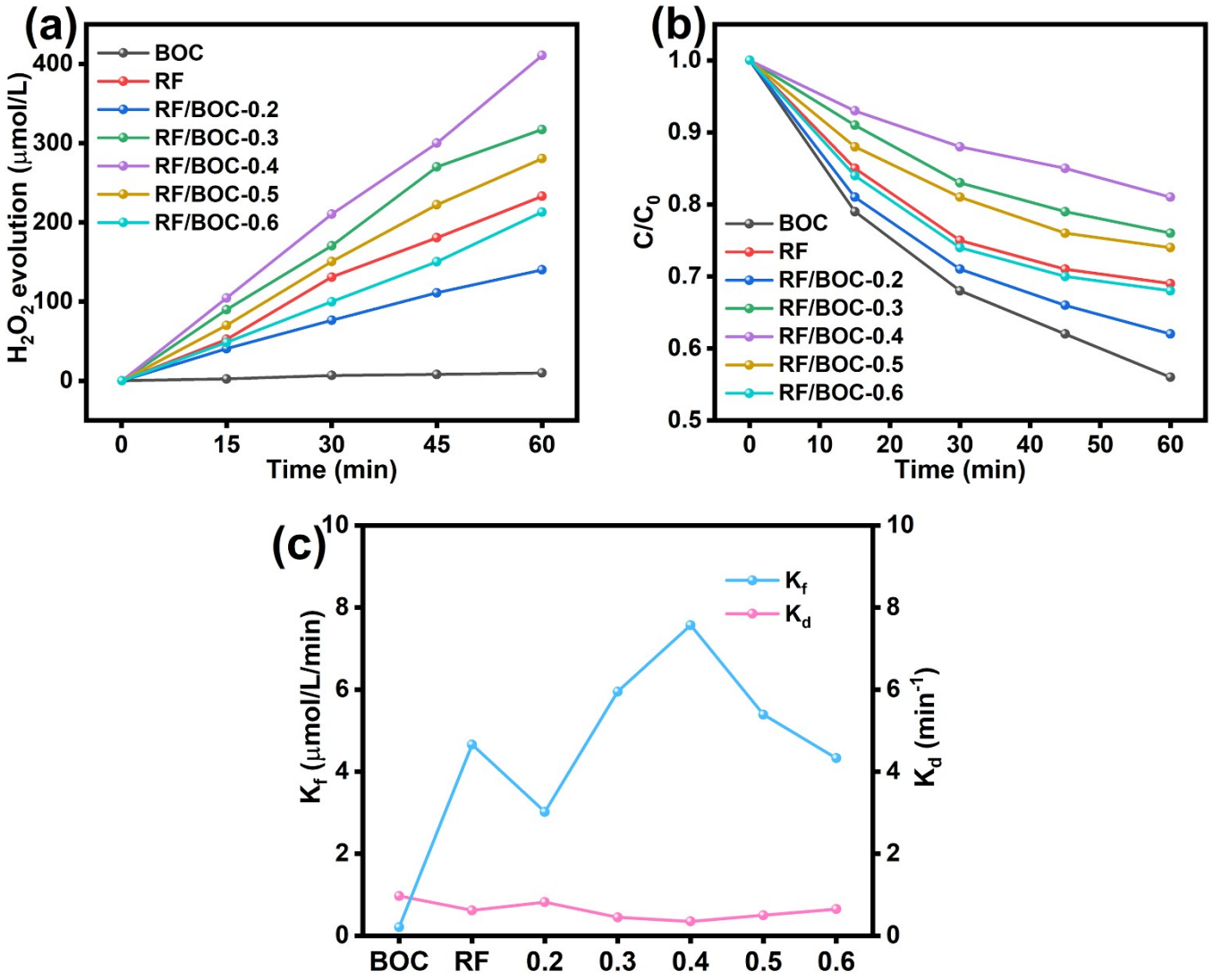

Fig. S5. (a) The generation of H_2O_2 using synthesized photocatalysts under light exposure. (b) Photocatalytic decomposition of H_2O_2 under light irradiation in an oxygen-free environment. (c) The formation rate constant (K_f) and decomposition rate constant (K_d) are associated with photocatalytic H_2O_2 production.

The decomposition rate of H_2O_2 for each sample was assessed (Fig. S5a) under oxygen-free conditions to isolate the effect of oxygen on overall H_2O_2 yield, given that H_2O_2 productivity is often hindered by rapid decomposition. As depicted in Fig. S5b, H_2O_2 decomposes more slowly on RF/BOC compared to pristine RF and BOC. To facilitate a direct comparison of photocatalytic activity, an empirical equation was used to model the H_2O_2 formation and decomposition profiles[18,19]. The formation rate constant (K_f) (μmol/L/min) and the decomposition rate constant (K_d) (min^{-1}) were derived (Fig. S5c). Notably, RF/BOC-0.4 exhibited the highest K_f and the lowest K_d, resulting in superior performance for H_2O_2 production.

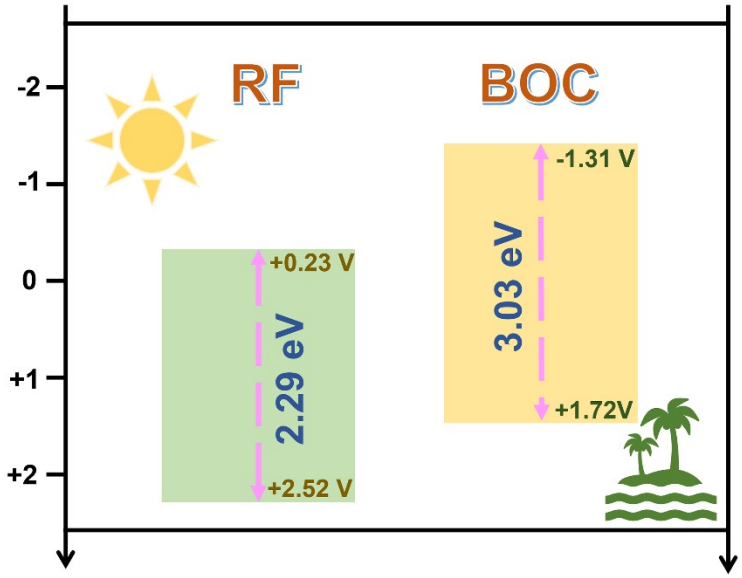

Fig. S6. The schematic illustration of band configuration of BOC and RF.

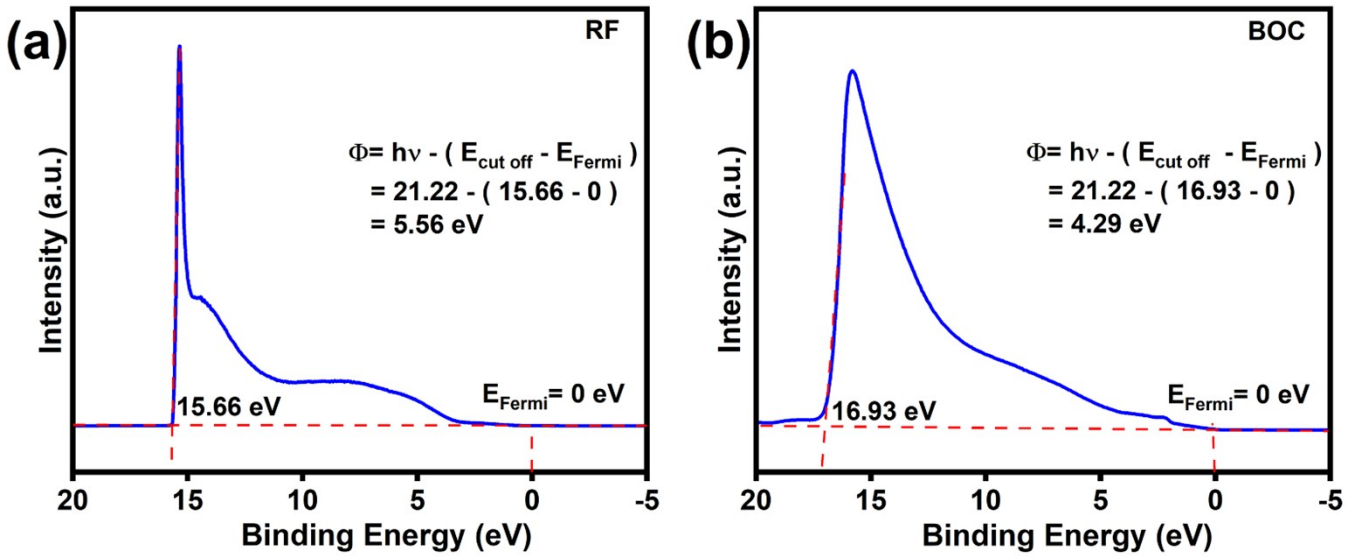

Fig. S7. The UPS of (a) RF and (b) BOC.

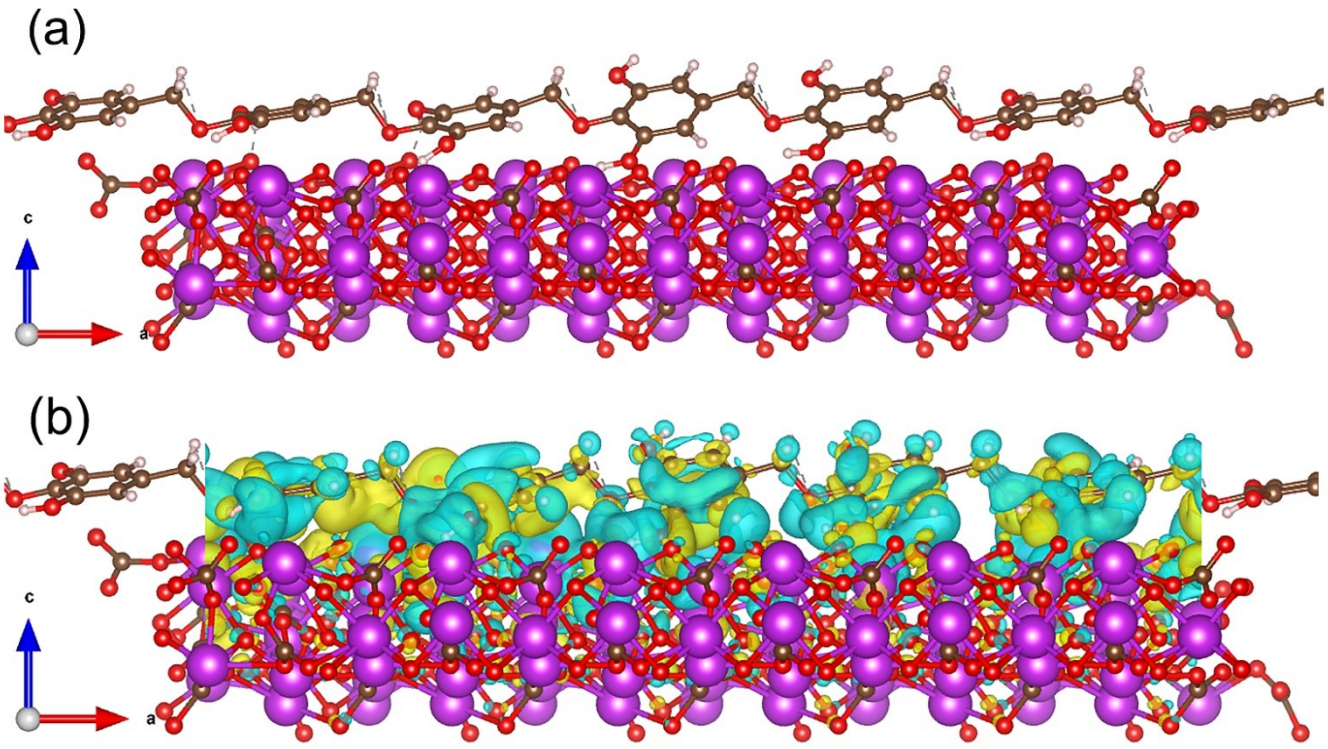

Fig. S8. (a) The optimized structure and (b) the side view of the charge density difference of RF/BOC heterostructure.

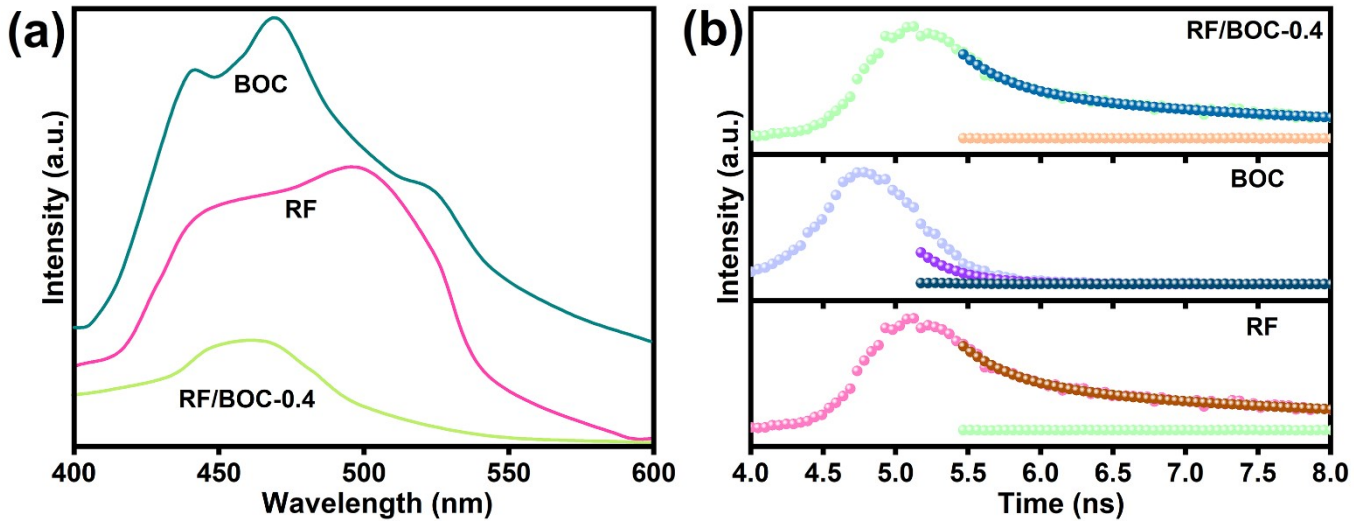

Fig. S9. (a) Photoluminescence (PL) emission spectra; (b) Time-resolved Photoluminescence (TRPL) spectra.

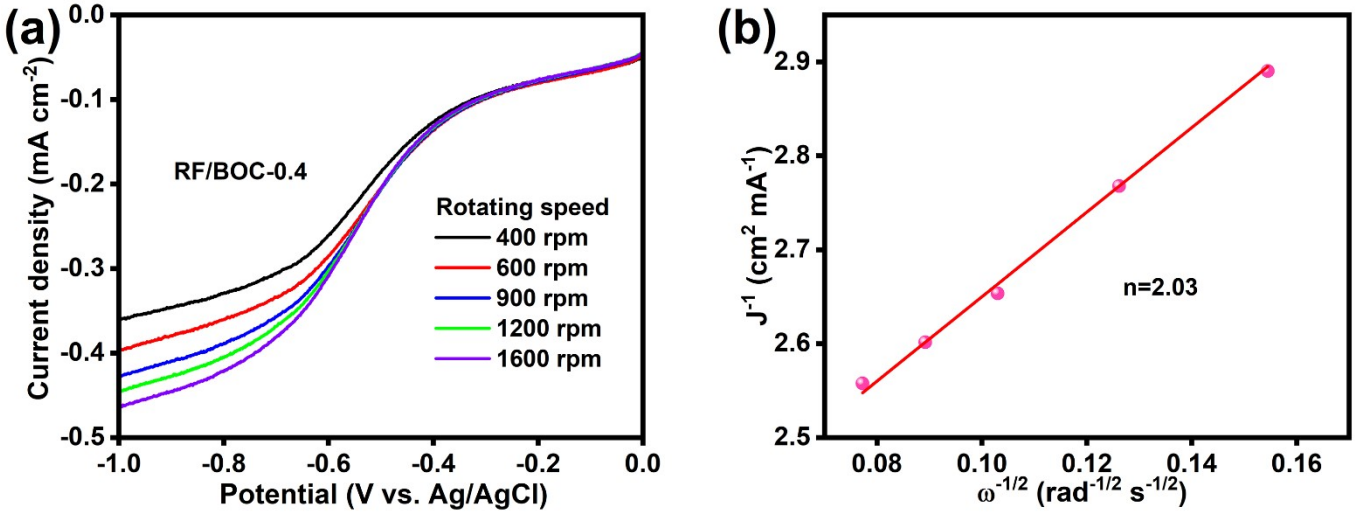

Fig. S10. (a) Linear-sweep RDE voltammogram of RF/BOC-0.4. (b) Koutecky-Levich (K-L) plots of RF/BOC-0.4. (0.1 M O_2-saturated Na_2SO_4 buffer solution (pH = 7) at different rotating speeds).

The rotating disk electrode (RDE) is tested using linear sweep voltammetry (LSV) as shown in Fig. S10a, the current density increases as the rotational speed rises. The current density in the examined sample consists of both diffusion-controlled and reaction kinetics-controlled regions. From the slope in Fig. S10b, the average electron transfer number during the O_2 reduction reaction is calculated to be 2.03, indicating that RF/BOC-0.4 participates in a two-electron oxygen reduction reaction (ORR) process.

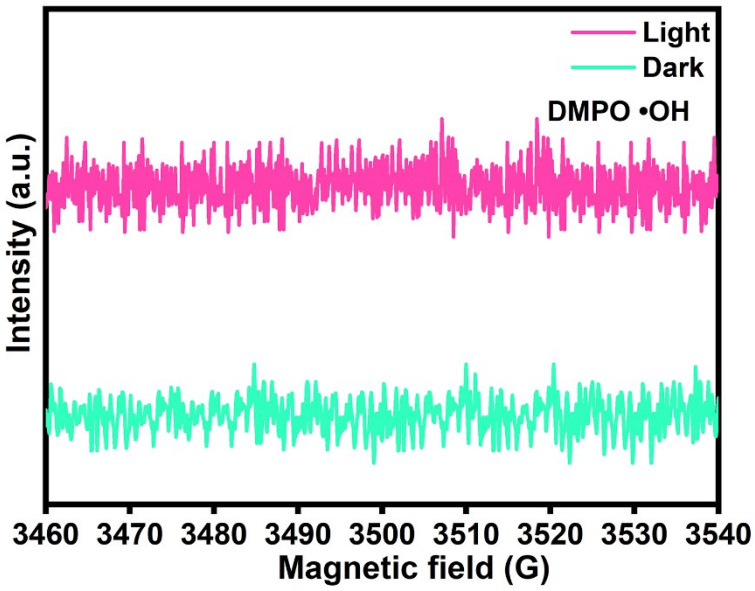

Fig. S11. EPR spectra under dark and simulated solar irradiation for DMPO •OH of RF/BOC-0.4.

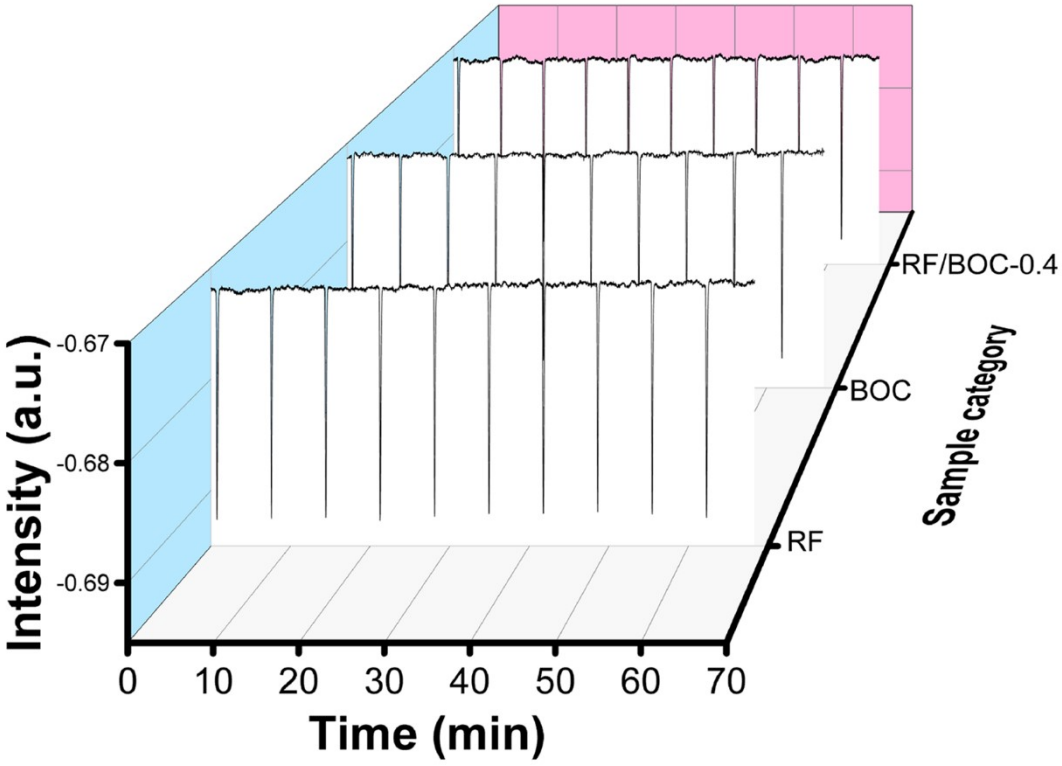

Fig. S12. Oxygen pulse adsorption experiments for RF, BOC, and RF/BOC-0.4.

The results shows that O_2 cumulative adsorbed quantity for RF, BOC, and RF/BOC-0.4 was $1.11*10^{-2}$, $2.6*10^{-3}$, $1.4*10^{-3}$ mmol/g, respectively. It indicated that the composite material RF/BOC-0.4 exhibited the lowest adsorption capacity, yet it still demonstrated favorable oxygen adsorption performance. This suggests that the photocatalytic activity is primarily influenced by the migration of electron-hole pairs within the heterogeneous junction structures. That is the excellent H_2O_2 production efficiency of RF/BOC-0.4 is more

dependent on the charge separation and transfer efficiency of the S-scheme heterojunction.

Table S1. Comparison of the photocatalytic H_2O_2 production performance.

Materials	Light source (nm)	Solvent system	H_2O_2 yield (μmol·h^{-1}·g^{-1})	Ref.
$ZnO/ZnIn_2S_4$	300 W Xe lamp	40 mL methanol	928	[20]
Au/WO_3	$\lambda \geq 420$ nm	4% CH_3OH in volume	240	[21]
AuCu- $BiVO_4$	420 nm LED lamp	Methanol	30.37	[22]
CN/SiW_{11}	Simulated sunlight	Methanol	178	[23]
$Au-WO_3$	$\lambda > 420$ nm	Methanol	108.8	[24]
HEP-TAPB-COF	$\lambda > 420$ nm	Methanol	990	[25]
$Ag_3PO_4(111)$	Simulated sunlight	Methanol	73.1	[26]
MIL-125/MIL-125-NH_2	Visible light	Methanol	38	[27]
NiO/CeO_2	300 W Xe lamp	Methanol	28.6	[28]

Table S2. $\tau_{Average}$ of samples RF, BOC, and RF/BOC-0.4.

Sample	τ_1	τ_2	A_1 (%)	A_2 (%)	τ_{Ave} (ns)	χ^2
RF	0.32	5.30	148.14 (88.54%)	1.14 (11.46%)	0.89	1.0513

BOC	0.39	3.71	1531.84 (97.40%)	4.26 (2.60%)	0.47	1.0848
RF/BOC-0.4	0.35	3.21	392.64 (9.53%)	411.88 (90.47%)	2.94	1.1956

References

1. J. Wang, Q. Chu, M. Xu, Y. Gong, Y. Feng, M. Meng and M. Gao, *Langmuir*, 2024, **40**, 15456-15467.
2. J. Wang, M. Xu, Q. Chu, Y. Gong, M. Gao, C. Sun, Y. Feng and X. Pu, *Applied Surface Science*, 2024, **670**, 160650.
3. G. Kresse and J. Furthmüller, *Computational Materials Science*, 1996, **6**, 15-50.
4. G. Kresse and J. Furthmüller, *Physical Review B*, 1996, **54**, 11169-11186.
5. J. P. Perdew, K. Burke and M. Ernzerhof, *Physical Review Letters*, 1996, **77**, 3865-3868.
6. G. Kresse and D. Joubert, *Physical Review B*, 1999, **59**, 1758-1775.
7. P. E. Blöchl, *Physical Review B*, 1994, **50**, 17953-17979
8. S. Grimme, J. Antony, S. Ehrlich and H. Krieg, *The Journal of Chemical Physics*, 2010, **132**.
9. X. Li, Q. Zheng, X. Wang, Q. Zheng, Y. Zhang, Y. Cong and S.-W. Lv, *Journal of Materials Chemistry A*, 2024, **12**, 8420-8428.
10. C. Zhao, X. Wang, Y. Yin, W. Tian, G. Zeng, H. Li, S. Ye, L. Wu and J. Liu, *Angewandte Chemie International Edition*, 2023, **62**, e202218318.
11. Y. Shiraishi, T. Takii, T. Hagi, S. Mori, Y. Kofuji, Y. Kitagawa, S. Tanaka, S. Ichikawa and T. Hirai, *Nature Materials*, 2019, **18**, 985-993.
12. M. Kawsar, M. Sahadat Hossain, S. Tabassum, N. M. Bahadur and S. Ahmed, *Nanoscale Advances*, 2024, **6**, 2682-2700.
13. H. Chu, R. Li, D. Zeng, W. Wang, B. Cui, T. Jia, L. Zhang and W. Wang, *Chemical Communications*, 2023, **59**, 14142-14145.
14. H. Zhang, Y. Zhu, Y. Sun, J. Khan, H. Liu, J. Xiao, H. Zhou and L. Han, *Journal of Environmental Chemical Engineering*, 2023, **11**, 111122.
15. K. Zhang, M. Dan, J. Yang, F. Wu, L. Wang, H. Tang and Z.-Q. Liu, *Advanced Functional Materials*, 2023, **33**, 2302964.
16. C. Zhao, X. Wang, Y. Yin, W. Tian, G. Zeng, H. Li, S. Ye, L. Wu and J. Liu, *Angewandte Chemie International Edition*, 2023, **62**, e202218318.
17. K. K. Das, U. A. Mohanty, R. Mohanty, P. P. Sarangi, D. P. Sahoo and K. Parida, *ACS Applied Energy Materials*, 2024, **7**, 6360-6375.
18. H. Kominami, K. Kamitani and A. Tanaka, *Chemical Communications*, 2024, **60**, 7017-7020
19. Y. Yang, J. Liu, M. Gu, B. Cheng, L. Wang and J. Yu, *Applied Catalysis B: Environment and Energy*, 2023, **333**, 122780
20. Y. Wu, Y. Yang, M. Gu, C. Bie, H. Tan, B. Cheng and J. Xu, *Chinese Journal of Catalysis*, 2023, **53**, 123-133.
21. Y. Wang, Y. Wang, J. Zhao and Y. Xu, *Applied Catalysis B: Environmental*, 2021, **299**, 120676.
22. K. Wang, M. Wang, J. Yu, D. Liao, H. Shi, X. Wang and H. Yu, *ACS Applied Nano Materials*, 2021, **4**, 13158-13166.
23. S. Zhao, X. Zhao, S. Ouyang and Y. Zhu, *Catalysis Science & Technology*, 2018, **8**, 1686-1695.
24. Y. Wang, Y. Wang, J. Zhao, M. Chen, X. Huang and Y. Xu, *Applied Catalysis B: Environmental*, 2021, **284**, 119691.

25. D. Chen, W. Chen, Y. Wu, L. Wang, X. Wu, H. Xu and L. Chen, *Angewandte Chemie International Edition*, 2023, **62**, e202217479.
26. X. Ma and H. Cheng, *Chemical Engineering Journal*, 2022, **429**, 132373.
27. X. Liao, W. Wei, Y. Zhou, M. Zhang, Y. Cai, H. Liu, Y. Yao, S. Lu and Q. Hao, *Catalysis Science & Technology*, 2020, **10**, 1015-1022.
28. P. Li, M. Zhang, X. Li, C. Wang, R. Wang, B. Wang and H. Yan, *Journal of Materials Science*, 2020, **55**, 15930-15944.